processes

MDPI

Article

Vibration Sample Augmentation Method Based on the TCV_CGAN Model for Turbine Blade Damage Detection

Jiamin Xu [1], Jianye Wang [1,*], Wangfan Li [1], Zhentian Wan [1], Xian Ding [1], Wangren Xu [1], Dongmei Dai [2] and Zhenxiang Liu [3]

[1] Shanghai Power Equipment Research Institute Co., Ltd., Shanghai 200240, China; xujiamin@speri.com.cn (J.X.); liwangfan@speri.com.cn (W.L.); wanzhentian@speri.com.cn (Z.W.); dingxian@speri.com.cn (X.D.); xuwangren@speri.com.cn (W.X.)
[2] Nanjing Boxiang Information Technology Co., Ltd., Nanjing 211800, China; njzjmeizi@163.com
[3] School of Energy and Environment, Southeast University, Nanjing 211189, China; lzq@seu.edu.cn
* Correspondence: wangjianye1@speri.com.cn

Abstract

The fault detection of steam turbine blades faces severe engineering challenges, such as insufficient fault data, imbalanced class distribution, and difficulty in extracting weak damage signal features, which seriously restrict the accuracy and generalization performance of intelligent diagnostic models. To solve the bottleneck problem of small samples mentioned above, a new time convolutional vector conditional generative adversarial network (TCV_CGAN) is proposed for data augmentation and damage detection of turbine blade. Firstly, multi-dimensional vector conditional encoding and stacked extended causal time convolution modules are integrated into an adversarial generation framework, and a composite loss function is constructed by combining adversarial loss and conditional matching loss. Based on the proposed TCV_CGAN, the controllable high fidelity vibration sample generation is obtained corresponding to different types of damage, degrees of damage, and rotational speed working conditions. In addition, the turbine blade damage detection framework is established based on the balanced augmented dataset generated from the TCV_CGAN, and it can improve the accuracy and reliability of damage detection for turbine blade. Moreover, the performance of the proposed method is analyzed and tested on an experimental turbine blade platform on sample augmentation and damage detection. The results indicate that the samples generated by TCV_CGAN maintained a high degree of distribution similarity and structural consistency with real vibration data with below 0.65 maximum mean difference and over 0.82 structure similarity index measure. In addition, the enhanced dataset significantly improved the effectiveness of blade damage detection at different speeds with the precision over 90% under all working conditions. The effectiveness and superiority of the proposed method are further verified through comparative analysis, which provides an effective data augmentation solution for fault diagnosis of small sample turbine blades.

Keywords: sample augmentation; turbine blade; vibration signals; damage detection; structural health monitoring

Check for updates

Academic Editor: Lifeng Wu

Received: 4 September 2026
Revised: 1 October 2026
Accepted: 15 October 2026
Published: 2 November 2026

Copyright: © 2026 by the authors. Licensee MDPI, Basel, Switzerland. This article is an open access article distributed under the terms and conditions of the Creative Commons Attribution (CC BY) license.

1. Introduction

By introducing a gas medium into the turbine to extract work, turbines are widely used in power equipment, such as aircraft engines, steam turbines, gas turbines and so on [1]. As a key power component of rotating machinery, turbine blades often work in extreme

environments of high temperature, high pressure, and high-speed rotation [2]. During long-term operation, fatigue cracks, wear, deformation and other damage defects are inevitable, which may lead to blade fracture and unit shutdown, causing huge economic losses and safety accidents [3]. Therefore, an accurate and efficient blade damage detection method is of great significance for turbine condition monitoring, fault warning, and remaining life prediction.

At present, damage detection of turbine blades is mainly carried out through various sensors, including vibration [4], strain [5], ultrasound [6], etc. Due to the advantage of real-time monitoring and simple deployment, vibration monitoring technology has become the main means of turbine blade damage detection [7]. The core of vibration-based blade damage detection is to explore subtle feature differences between healthy and damaged blades through signal analysis and deep learning models. However, the collection of damage vibration data for turbine blades faces prominent bottlenecks due to the limitations of actual industrial working conditions [8]. Specifically, the probability of blade damage is low, and the number of measured damage vibration samples is far less than that of healthy samples, resulting in a serious imbalance in the dataset [9]. In addition, most damage signals of turbine blades are weak and easily overwhelmed by noise and environmental interference, which affects the quality and quantity of monitoring vibration samples. Moreover, there are various types and degrees of blade damage, and it is difficult to cover all conditions, which makes the detection model prone to overfitting and poor generalization ability during training and testing [10].

Fortunately, data augmentation methods have been proposed as an effective approach to solving the problem of small and imbalanced mechanical fault samples [11]. Traditional vibration signal augmentation methods include time-domain translation, amplitude scaling, noise superposition, wavelet transform, and other physical transformation methods [12]. These methods are simple to operate, but only perform surface data conversion, which makes it difficult to explore the deep time series correlation and fault feature distribution. The fidelity of the generated samples is low, with limited improvement for model performance. In recent years, generative adversarial networks (GAN) have been widely used in sample generation due to their powerful unsupervised feature learning and data distribution fitting capabilities [13]. Nayak et al. [14] provided a comprehensive overview of the structure, variants, applications, and current work of GANs. Lin et al. [15] proposed an improved GAN model for machinery fault diagnostics under data imbalance, which can improve the generated sample quality under limited data.

To realize controlled generation, the conditional GAN (CGAN) is presented by adding label constraint conditions on the basis of traditional GAN, which can make up for the blindness of original GAN generation [16]. Wang et al. [17] presented the temporal denoising diffusion CGAN model for accurate synthesis of different fault samples by integrating the class-conditional generation mechanism. Wu et al. [18] developed a data augmentation method by combining the genetic algorithm and Wasserstein CGAN to solve the challenges of insufficient data collection and limited availability of labeled samples for bearing faults. Nevertheless, existing generation methods for time-series fault signals still have two prominent technical bottlenecks. On the one hand, traditional CGAN and its variants mostly adopt ordinary convolution structures and single discrete label constraints [19], which cannot capture the long-range temporal dependence of vibration signals, and the rough label supervision easily leads to conditional confusion and invalid cross-condition generation. On the other hand, TCN-GAN methods only use temporal convolution to optimize the feature extraction ability, which lacks a multi-dimensional conditional control mechanism for damage attributes and working conditions. It is difficult to realize fine-grained directional generation for turbine blades with multiple damage types, damage degrees and operating

speeds. Therefore, none of the existing methods can simultaneously solve the two core problems of temporal feature extraction of vibration signals and controllable generation under multi-parameter conditions, which greatly limits the effect of sample augmentation in turbine blade damage detection.

These practical bottlenecks are widely recognized in rotating-machinery fault-diagnosis research, as pointed out in [20]. It stressed that synthetic sample augmentation should be comprehensively assessed by both signal-level indicators and downstream classification performance under multiple working-condition scenarios. To address the aforementioned shortcomings, the time convolutional networks (TCN) and vector conditional constraints are integrated into CGAN to construct a TCV_CGAN model, which is implemented for turbine blade damage detection. Specifically, the TCN module is employed to capture the long-distance time-series dependence of blade vibration signals, and the CGAN is used to generate a large number of high-quality samples to address the data imbalance problem. Based on the vector conditional mechanism, accurate classification and directional generation are realized for turbine blades with different damage. Through the experimental platform of turbine blades, the performance of the proposed method is tested under different conditions. The main contributions are summarized as follows:

(1) By combining temporal convolution feature extraction with conditional adversarial generation, the TCV_CGAN model is proposed to realize high-fidelity generation of vibration signals and damage detection for turbine blades.
(2) The vector multi-condition constraint mechanism is designed to associate damage type, damage degree and working condition parameters, which improves the pertinence and diversity of augmented vibration samples.
(3) The turbine blade experimental platform is established to validate the proposed method on sample augmentation and damage detection, which is employed to verify its detection accuracy and generalization ability based on comparative methods.

The remainder of this research is organized as follows. Section 2 describes the related works, and Section 3 details the proposed TCV_CGAN for turbine blade damage detection. In addition, the experimental platform construction and testing are presented in Section 4, including the results and discussion with comparative analyses. Finally, Section 5 concludes the research.

2. Related Works

2.1. Temporal Convolutional Network

TCN is a specialized convolutional architecture for long-sequence time-series signals, which effectively compensates for the defects of traditional convolutional neural networks (CNNs) in temporal feature extraction and recurrent neural networks (RNNs) in recursive gradient vanishing and low efficiency [21]. TCN adopts a composite structure of causal convolution, dilated convolution and residual connection, which can extract long-distance temporal dependence of vibration signals, while strictly ensuring time-domain causality and feature integrity [22].

Specifically, the causal convolution is the basic guarantee for the time-series validity of TCN. For one-dimensional vibration time-series data, the output of any time step t only depends on the input of current and historical time steps (0–t). It completely avoids future information leakage, which is highly consistent with the physical sampling characteristics of vibration signals.

Dilated convolution is the core module to expand the receptive field without increasing network parameters. By setting a dilation factor d, the convolution kernel interval is expanded to capture long-range correlation features of vibration. It is expressed as

$$y(t) = \sum_{k=0}^{K-1} f(k)x(t - d \cdot k), \tag{1}$$

where $y(t)$ is the output feature at time step t, $x(.)$ is the original signal, $f(k)$ is the weight of the k-th convolution kernel, K is the kernel size, and d is the dilation factor.

The effective receptive field of a multi-layer stacked TCN determines the maximum time-series range that the model can perceive, and it is calculated as

$$R = (K - 1)\sum_{i=0}^{n-1} d_i + 1, \tag{2}$$

where n is the number of TCN layers, and d_i is the dilation factor of the i-th layer.

Exponentially increasing dilation factors enable TCN to obtain an ultra-large receptive field, capturing both local fault pulse features and global time-domain variation in vibration signals. In addition, the residual connection is introduced into the TCN to solve the performance degradation problem of deep networks [23]. The residual block realizes cross-layer feature fusion through identity mapping, and it is expressed as

$$H_{out} = F(H_{in}) + H_{in}, \tag{3}$$

where H_{in} is the input residual block, $\mathrm{F}(.)$ represents the composite transformation of dilated convolution, batch normalization and activation function, and H_{out} is the final output.

2.2. Conditional Generative Adversarial Network

CGAN is an improved variant of the original GAN, which solves the problem of unconstrained and blind generation of traditional GAN by introducing explicit conditional constraint variables. The core innovation lies in integrating label information and attribute parameters into the adversarial training process of the generator and discriminator, realizing directional and controllable generation of target samples [24].

Different from the GAN, both the generator G and discriminator D of CGAN take the conditional variable c as auxiliary input. The G fuses random Gaussian noise z and conditional feature c to produce simulated samples $G(z|c)$, and the D simultaneously evaluates the authenticity of input samples, forming a constrained adversarial game. Based on the minimax game theory, the standard CGAN objective function is defined as:

$$\min_G \max_D V(D, G) = E_{x-Pdata(x)}[\log D(x|c)] + E_{z-Pz(z)}[\log(1 - D(G(z|c)|c))], \tag{4}$$

where $Pdata(x)$ denotes the distribution of real samples, $Pz(z)$ represents the distribution of random latent noise, $E(.)$ is the mathematical expectation operator, $D(x|c)$ is the probability output of the discriminator for real samples under conditional constraint c, and $G(z|c)$ refers to the fake samples generated by the condition-guided generator.

During iterative training, the D maximizes the objective function to distinguish real measured data and synthetic samples, while the G minimizes the objective function to narrow the distribution gap between generated and real samples. Finally, the model achieves Nash equilibrium, and the G can stably output conditional samples. Nevertheless, traditional CGAN generally adopts single discrete label constraints and ordinary convolution structures, which cannot capture long-range time-series dependencies of signals.

3. The Proposed Method

3.1. Overall Framework of the Proposed TCV_CGAN

To solve the problems of insufficient temporal feature extraction for time-series vibration signals, the TCV_CGAN is proposed for vibration sample augmentation and turbine blade damage detection. Different from existing generation models, the proposed TCV_CGAN integrates multi-dimensional vector conditional encoding and multi-scale temporal convolution feature extraction into the adversarial generation framework, which can realize controllable, high-fidelity and fine-grained generation of multi-degree blade damage vibration samples.

The overall architecture of TCV_CGAN consists of three core functional modules, including a multi-dimensional vector conditional encoding module, a temporal convolution-based generator (TC-Generator), and a conditional discriminator. As shown in Figure 1, the complete workflow is as follows:

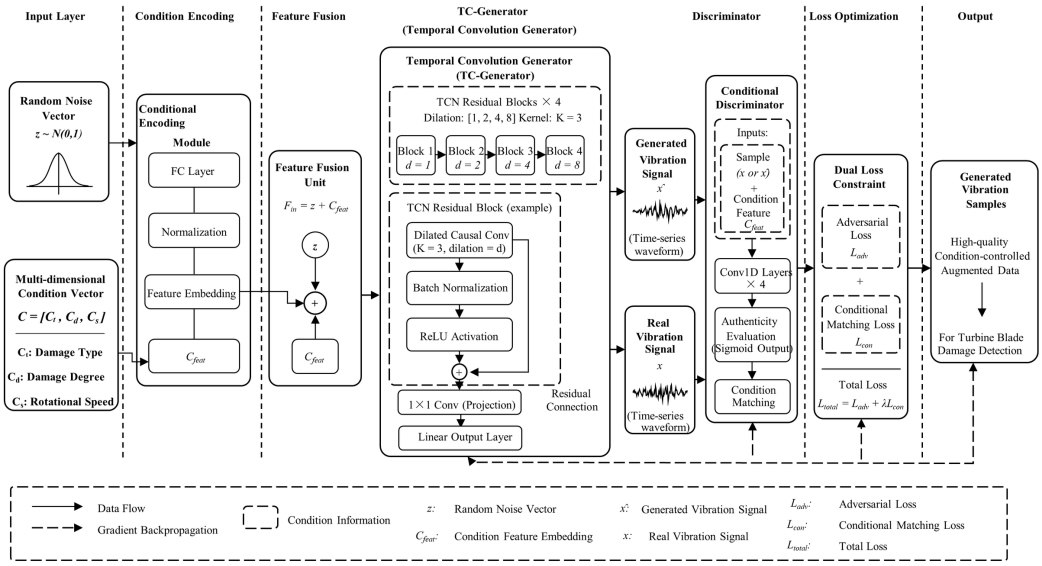


Figure 1. The workflow of the proposed TCV_CGAN.

Firstly, the multi-dimensional damage attributes and working conditions are normalized and encoded to obtain standardized conditional feature embedding. By fusing the conditional embedding with Gaussian latent noise, the long-range time-series vibration features are extracted through stacked dilated causal convolution blocks, which can generate simulated vibration signals. In addition, the real vibration samples and generated samples with conditional labels are input into the D to complete adversarial optimization combining authenticity discrimination. After iterative training converges the model, the G outputs reliable augmented vibration samples for turbine blade damage detection.

Different from existing TCN-GAN that only replaces partial convolution layers with TCN, the generator of TCV_CGAN completely takes stacked dilated causal TCN residual blocks as the full backbone, ensuring the full-length receptive field of vibration sequences and strict time-domain causality. More importantly, differing from traditional CGAN that only relies on single-label implicit supervision, TCV_CGAN deeply couples the multi-dimensional vector conditional encoding module with the TCN generator at the feature level, and constructs a dual-constraint loss mechanism. This design enables the model to simultaneously achieve high-fidelity generation of time-series waveforms and accurate matching of damage-working condition attributes, which is the core difference between the proposed method and existing generation models.

3.2. Multi-Dimensional Vector Conditional Encoding Module

Generally, the traditional CGAN only adopts a single discrete label condition, which cannot characterize the complex attribute characteristics of turbine blade damage. To achieve fine-grained controlled generation, a joint condition vector containing three attribute dimensions is constructed to characterize the complex damage attributes and working conditions of turbine blades, including damage type, damage degree and rotational speed. It is expressed as

$$C = [C_t, C_d, C_s] \in \mathbb{R}^3, \tag{5}$$

where C_t denotes the damage type label, C_d denotes the damage degree label, C_s denotes the blade operating rotation speed parameter.

Among them, C_s is a continuous physical parameter, which is normalized to $[0, 1]$ with an encoded dimension of 1. In addition, C_t and C_d are discrete categorical variables encoded by one-hot encoding. In the current experimental scenario, only crack damage is set for verification, so C_t contains 1 category with an encoded dimension of 1, where C_d contains 4 categories (health, slight crack, moderate crack, severe crack) with an encoded dimension of 4. After feature splicing, the initial numerical dimension of the condition vector is 6. The feature mapping is expressed as:

$$Hot(x_i) = [T(x_i = 1), T(x_i = 2), \ldots, T(x_i = N)], \tag{6}$$

where N is the total number of categories, $T(.)$ is the indicator function. If the condition is true, the value $T(.)$ is 1; otherwise, it is 0.

For the C_s, the continuous speed is normalized, and it is calculated as

$$\widehat{C}_s = \frac{C_s - C_{s,\min}}{C_{s,\max} - C_{s,\min}}, \tag{7}$$

where $C_{s,min}$ and $C_{s,max}$ represent the minimum and maximum rotational speed in the working condition, respectively.

After discrete encoding and continuous normalization, the conditional vector is mapped to the high-dimensional feature space consistent with the vibration signal through two fully connected (FC) layers. The feature mapping is expressed as:

$$C_{feat} = \sigma[W_2 \cdot \sigma(W_1 \cdot C + b_1) + b_2], \tag{8}$$

where W_1, W_2 are weight matrices, $b1$, $b2$ are bias terms, σ denotes the ReLU activation function, and C_{feat} is the final conditional embedding feature for subsequent fusion with noise features.

3.3. Temporal Convolution-Based Generator

Aiming at the problem that ordinary convolution cannot capture long-range time-series dependence of vibration signals, the G of the proposed TCV_CGAN is completely constructed based on stacked TCN residual blocks. It employs dilated causal convolution to ensure time-domain causality and expand the receptive field. The G takes the fused feature of latent noise and conditional embedding as input, and outputs one-dimensional vibration samples with the same length as real measured signals, as shown in Figure 2.

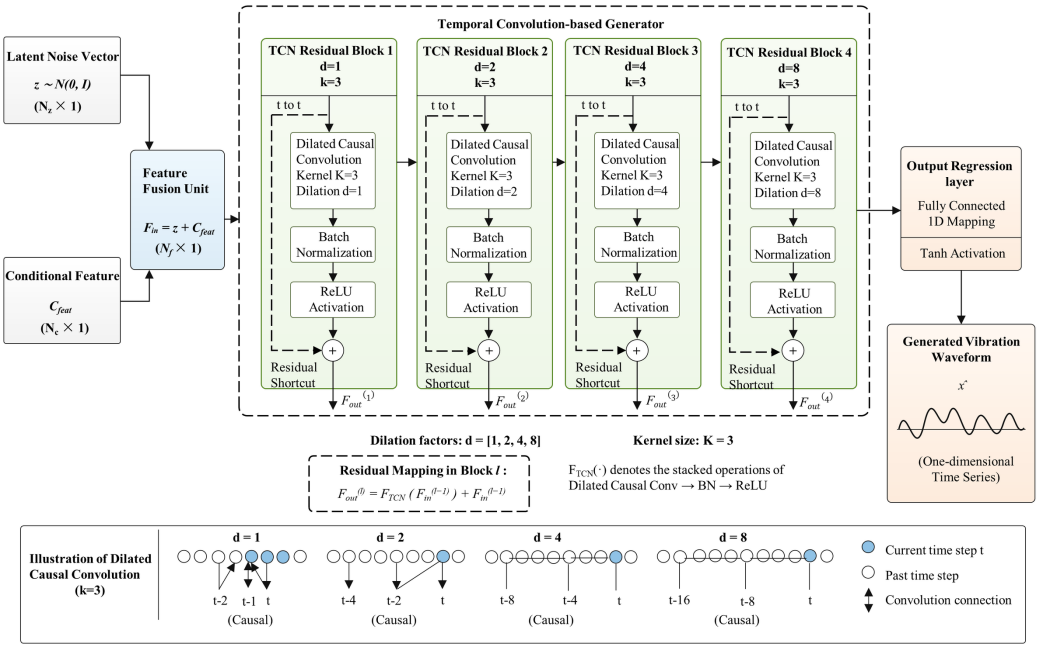


Figure 2. The structure of the temporal convolution-based generator.

The latent noise vector is defined as $z \sim N(0, 1)$, which obeys a standard Gaussian distribution. The fusion process of noise feature and conditional feature is element-wise addition, and it is expressed as

$$F_{in} = z + C_{feat}, \tag{9}$$

where F_{in} is the input feature of the generator network.

The G contains 4 cascaded TCN residual blocks, and each block contains dilated causal convolution, batch normalization and ReLU activation. The dilation factors are set as $d = [1, 2, 4, 8]$ in turn, and it can realize exponential expansion of the receptive field. Combined with the TCN basic, the output of a single-layer dilated causal convolution is expressed as

$$F_{out}(t) = \sum_{k=0}^{K-1} f(k) F_{in}(t - d \cdot k), \tag{10}$$

where the convolution kernel size K is 3.

According to Equation (2), the final effective receptive field of the generator is 31 time points. With a sampling frequency of 2560 Hz, this receptive field corresponds to a time width of approximately 12 ms, which can completely cover the rising edge, peak value and attenuation segment of the blade crack impact pulse. This configuration ensures that each output point of the generated signal perceives sufficient local fault temporal features, and the whole generated sequence maintains complete structural characteristics of real vibration signals through the continuous causal convolution process. In addition, the residual connection in the TCN block avoids network degradation during deep training, and the residual mapping is expressed as

$$F_{res} = F_{TCN}(F_{in}) + F_{in}, \tag{11}$$

where $F_{TCN}(.)$ represents the composite transformation of convolution, normalization and activation.

After multi-layer TCN feature extraction, the final vibration sample is output through the activation function layer, and it is expressed as

$$\widehat{x} = \tanh(F_{res,final}), \tag{12}$$

where $\widehat{x}$ is the generated turbine blade vibration sample.

3.4. Conditional Discriminator and Composite Loss Function

The D of the proposed TCV_CGAN adopts a conditional joint discrimination mechanism, which takes sample features and conditional embedding features as joint input. It can judge sample authenticity and condition matching degree simultaneously. Different from the D of the traditional model, it not only distinguishes real and fake samples, but also restricts the generated samples to match the present damage conditions, eliminating invalid heterogeneous samples.

The D first fuses the input sample $x/\widehat{x}$ and conditional feature C_{feat} through channel splicing. It is expressed as

$$F_D = Concat(x, C_{feat}), \tag{13}$$

Then, the fused features are extracted through four layers of one-dimensional convolution, and the final probability score is output through the sigmoid function to judge the authenticity of the sample. To ensure stable training and high-quality generation, a multi-component composite loss function is constructed, including basic adversarial loss and conditional matching loss. The total loss is defined as

$$L_{total} = L_{adv} + \lambda L_{con}, \tag{14}$$

where L_{adv} is the adversarial loss, L_{con} is the conditional matching loss, and λ is the balance coefficient of the conditional loss.

(1) Adversarial loss L_{adv}

Different from image generation tasks, turbine blade vibration signals are typical continuous time-series data with strong temporal correlation and fault-sensitive pulse characteristics. Based on the classic CGAN minimax game theory, the adversarial loss is further optimized and adapted for one-dimensional vibration sequence generation. This loss aims to narrow the overall distribution gap between real measured and synthetic samples, which drives the G to learn the inherent time-frequency statistical characteristics of real blade damage signals. The optimized adversarial loss function for TCV_CGAN is defined as

$$L_{adv} = E_{x-Pdata(x)}[\log D(x|C)] + E_{z-Pz(z)}[\log(1 - D(G(z|C)|C))], \tag{15}$$

where $x{\sim}Pdata(x)$ denotes the represents the real vibration samples, $z{\sim}Pz(z)$ is the standard Gaussian noise input, and C denotes the multi-dimensional vector condition containing damage type, damage degree and operating speed.

The D maximizes the log-likelihood of distinguishing real samples and generated samples under specific conditional constraints, while the G minimizes the objective function to fool the discriminator. Through an iterative two-player adversarial game, the G can gradually fit the real vibration data distribution and produce visually and statistically reasonable time-series waveforms.

(2) Conditional matching loss L_{con}

Traditional CGAN only relies on implicit label supervision in adversarial loss, which cannot guarantee the strict matching between generated sample features and preset damage conditions. It easily causes conditional confusion, label disorder and cross-condition invalid generation, especially for multi-type and multi-degree blade damage generation tasks. To solve this problem, an explicit feature-level conditional matching loss is introduced based on L2 norm distance. This loss imposes hard constraints on the generated samples from the feature dimension, forcing the synthetic vibration features to be highly consistent with the input conditional embedding C_{feat}. The conditional matching loss is calculated as

$$L_{con} = \left\| Feature(G(z|C)) - C_{feat} \right\|_2^2, \tag{16}$$

where $Feature(.)$ denotes the high-dimensional feature vector extracted from the last hidden layer of the G. It represents the essential time-series fault characteristics of the generated vibration sample.

By minimizing the Euclidean distance between generated features and conditional features, the model realizes fine-grained supervised generation. This explicit constraint fundamentally eliminates the phenomenon of mismatched damage attributes and disordered working conditions in traditional models. It significantly improves the attribute accuracy and usability of augmented blade vibration samples.

In summary, the dual-supervision mechanism of adversarial loss and conditional matching loss enables TCV_CGAN to simultaneously satisfy distribution authenticity and conditional attribute accuracy, which provides a solid mathematical guarantee for high-quality and controllable augmentation of turbine blade multi-damage vibration samples.

3.5. Turbine Blade Damage Detection Based on TCV_CGAN Augmentation

Based on the TCV_CGAN vibration sample augmentation, the turbine blade damage detection method is proposed to effectively solve the small-sample and class-imbalanced problems in actual conditions. The entire detection process is divided into four stages, including signal pre-processing, data augmentation, model training, and damage detection, as shown in Figure 3.

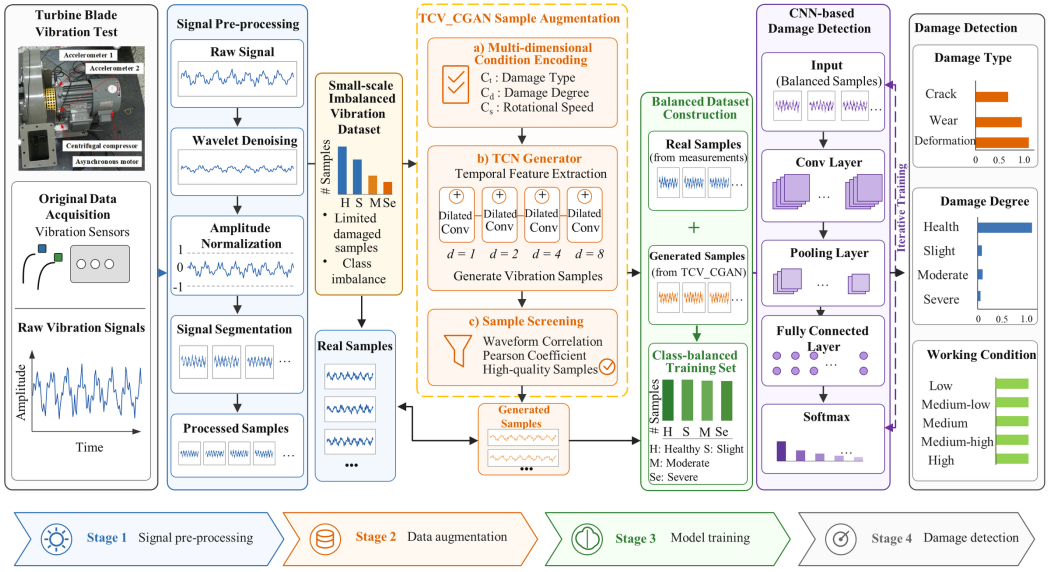


Figure 3. The process of the proposed method.

(1) Signal pre-processing: The original turbine blade vibration signals contain environmental noise and redundant interference information, which need standardized pre-processing before model training, including signal denoising, amplitude normalization and time-series segmentation. Firstly, wavelet threshold denoising is adopted to eliminate Gaussian noise and impulse noise in the original signal, and it is defined as

$$\widehat{W}_{j,k} = sign(W_{j,k})(|W_{j,k}| - T)_+, \tag{17}$$

where $W_{j,k}$ denotes the original wavelet decomposition coefficient, $\widehat{W}_{j,k}$ is the denoised coefficient, T is the set threshold, and $(.)+$ represents the positive value retention operation. Subsequently, the denoised signal is normalized to unify the amplitude distribution range and eliminate the influence of voltage fluctuation of the acquisition equipment. It is expressed as

$$x_{norm} = \frac{x - x_{\min}}{x_{\max} - x_{\min}}, \tag{18}$$

where x is the original vibration sequence, x_{max} and x_{min} are the maximum and minimum values of the original signal amplitude, respectively.

Finally, the long-time vibration sequence is segmented into equal-length sample units to adapt to the input dimension of TCV_CGAN and the detection model.

(2) Data augmentation: Based on the pre-processed small-scale real dataset, the TCV_CGAN model is used for directional sample augmentation. To ensure the quality of augmented data, a single-index sample screening mechanism based on waveform correlation is adopted to eliminate low-fidelity invalid samples. Specifically, the Pearson correlation coefficient is used to quantitatively evaluate the waveform similarity between each generated sample and real samples under the same damage condition and rotational speed. This index reflects the consistency of overall vibration trend, fault pulse position and morphological characteristics. Since all vibration signals are normalized to a uniform amplitude range in the preprocessing step, the Pearson correlation coefficient can also indirectly reflect the matching degree of amplitude characteristics to a certain extent [25]. It is expressed as

$$p(\widehat{x}, x) = \frac{COV(\widehat{x}, x)}{\sqrt{D(\widehat{x})}\sqrt{D(x)}}, \tag{19}$$

where $Cov(.)$ is the covariance, $D(.)$ is the variance.

For each generated sample, we calculate pairwise Pearson correlation coefficients against all real samples from the same working condition, and take the average value as its quality score. Only generated samples with an average Pearson correlation coefficient ≥ 0.85 (The value can be changed for different conditions) are retained for constructing the balanced augmented dataset. Samples with an average value below this threshold are removed as low-fidelity invalid samples.

(3) Model training: The generated samples are fused with real measured samples to construct a balanced turbine blade damage dataset, which solves the problem of an unbalanced quantity of healthy samples and various damage samples. Taking the classical CNN models as the basic detection network, the balanced augmented dataset is input for iterative training.

(4) Damage detection: After the detection model converges, the real turbine blade vibration test samples are input into the trained network to realize automatic blade damage detection for turbines. Combined with multiple evaluation indices including accuracy, precision, recall and F1-score, the detection performance is comprehensively verified. Meanwhile, by comparing the detection results of the original small-sample dataset and the traditional augmentation dataset, the superiority of the proposed method is further demonstrated.

4. Results and Discussion

4.1. Experimental Dataset

To verify the proposed method, considering the difficulty of constructing a steam turbine long blade test rig, the experimental platform is constructed for simulated turbine blade damage detection, as shown in Figure 4.

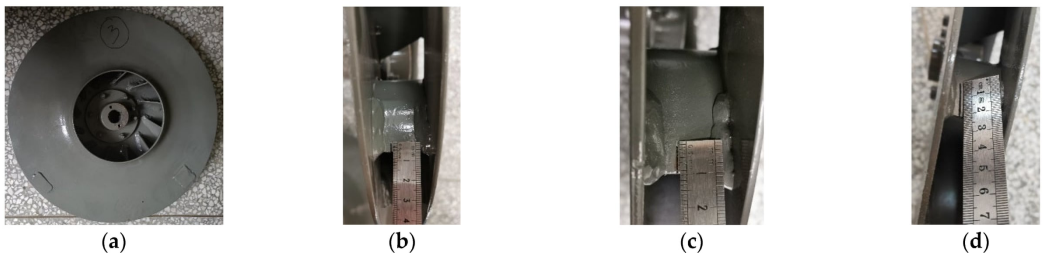
The vibration response of turbine blades is captured by two high-sensitivity vibration sensors installed at different spatial positions on the surface of the turbine, which can effectively obtain multi-point vibration information and ensure the comprehensiveness and authenticity of the collected signal data. The entire experimental testing system mainly consists of a turbine, standard test blades, a precision speed controller, and dual

vibration sensing units. The turbine system runs stably at five speeds, including 1200 rpm, 1500 rpm, 1800 rpm, 2100 rpm, and 2400 rpm. It can verify the generalization and detection performance of the proposed method in different working scenarios.



Figure 4. The overall layout and structural composition of the experimental platform.

Considering the convenience of processing and accurate quantification, wire cutting is used to simulate blade crack damage. To analyze the varying degrees of crack damage on the blades, four different lengths of cracks are set on one of the sub blades, including 0 mm (health), 5 mm (slight), 10 mm (moderate), and 20 mm (severe) cracks. The crack width is 1 mm and the thickness is 2.5 mm, completely penetrating the inner and outer surfaces of the blade. The conditions of cracked blades are shown in Figure 5.



(**a**) (**b**) (**c**) (**d**)

Figure 5. The crack condition of turbine blade: (**a**) Health. (**b**) Slight. (**c**) Moderate. (**d**) Severe.

Two unidirectional piezoelectric acceleration sensors (608A11, PCB Piezotronics, NY, USA) are employed to collect vibration signals, which are installed at different positions near the casing. One is near the output end, and the other is opposite to sensor 1. To ensure consistency and comparability in the signal processing process, the sampling frequency of the two vibration sensors is 2560 Hz, and each signal is recorded for one second.

In actual operation, the sample size of normal blades is larger than that of damaged blades. As the blade damage worsens, the sample size decreases. Therefore, under each operating condition, 100 sets, 30 sets, 20 sets, and 10 sets of four types of blades are collected to form an unbalanced sample of turbine blade damage. Finally, the dataset contains four blade crack lengths, namely 0 mm, 5 mm, 10 mm, and 20 mm, which are assigned labels 0, 1, 2, and 3 for easy supervised classification. Meanwhile, the blades are tested under five working conditions: 1200 rpm, 1500 rpm, 1800 rpm, and 2100 rpm, representing the rotational speed of the machine. This unbalanced dataset includes a total of 2 sensors, 4 crack lengths, 5 working conditions, and different blade damage vibration samples. To construct a balanced training dataset, TCV_CGAN generates additional samples for minority fault classes. Generated samples are only incorporated into the training set and never participate in testing. The full statistics are summarized in Table 1.

Table 1. The composition of the unbalanced experimental dataset.

Label	Crack Length	Sensors	Raw Samples	Training Samples	Testing Samples	Generated Augmented Samples	Working Conditions
0	0 mm	Sensor 1	100	70	30	0	1200 rpm 1500 rpm 1800 rpm 2100 rpm 2400 rpm
0	0 mm	Sensor 2	100	70	30	0	
1	5 mm	Sensor 1	30	21	9	49	
1	5 mm	Sensor 2	30	21	9	49	
2	10 mm	Sensor 1	20	14	6	56	
2	10 mm	Sensor 2	20	14	6	56	
3	20 mm	Sensor 1	10	7	3	63	
3	20 mm	Sensor 2	10	7	3	63	

According to the standard 70 and 30 training test segmentation, covering all four crack severity categories. Every second of vibration recording is considered an independent sample. Under each working condition, each crack length blade has its own number of samples. Since all samples are collected independently, there is no time overlap or data leakage between the training and testing sets, as shown in Table 2.

All quantitative experimental results in this study are averaged from 10 independent repeated runs. For each run, the network parameters are randomly initialized and the training samples are re-shuffled to eliminate the influence of random factors and ensure the stability and reproducibility of the results. To decouple the effects of rotational speed and crack size, the control variable method is adopted in the experimental design. When analyzing crack characteristics, the rotational speed is kept constant and only the crack length is changed. In addition, when testing speed robustness, the crack conditions are fixed and only the rotational speed is adjusted. In this way, the vibration characteristics caused by crack size and rotational speed were effectively separated. The model has been trained to recognize features related to cracks, rather than amplitude changes related to velocity, ensuring that the detection results mainly reflect the severity of cracks.

Table 2. The composition of the training and testing dataset for different cracked blades.

Label	Crack Length	Training Samples	Testing Samples	Working Conditions
0	0 mm	2 × 70	2 × 30	1200 rpm, 1500 rpm 1800 rpm, 2100 rpm 2400 rpm
1	5 mm	2 × 21	2 × 9	
2	10 mm	2 × 14	2 × 6	
3	20 mm	2 × 7	2 × 3	

Each individual vibration sample is defined as a continuous 1 s time series with 2560 data points (corresponding to the sampling frequency of 2560 Hz), and all samples are segmented with no time overlap. Two vibration sensors collect data synchronously, and each sensor produces an independent sample set. All samples are derived from multiple independent experimental runs. For each damage degree at each rotational speed, multiple independent start-stop experiments were carried out. The training set and test set come from completely separate experimental batches without any shared data, to avoid data leakage and ensure objective performance evaluation.

4.2. The Result of Sample Augmentation

To visually demonstrate the quality of the signal generated by the proposed method, original and generated samples of four different lengths of crack-damaged blades are selected at a 1500 rpm condition, as shown in Figure 6.

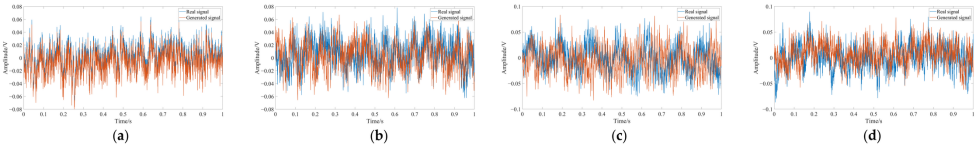


Figure 6. Original and generated samples of four different crack lengths: (**a**) Health. (**b**) Slight. (**c**) Moderate. (**d**) Severe.

Obviously, the generated samples are highly consistent with the original samples in all four crack scenarios. The curves of the generated data and the original data have similar overall trends, indicating that the proposed model can well preserve the characteristics of turbine blade vibration. Meanwhile, the generated samples do not simply replicate the original samples, but exhibit moderate interference and differences, reflecting a certain degree of data diversity. The results indicate that the proposed method can introduce controllable offset while maintaining the same type of structural prior, generating samples that are highly consistent with real samples and have a certain degree of variability. This provides a more representative data foundation for turbine blade damage detection.

To quantitatively evaluate the sample generation performance of the proposed method, two evaluation metrics are used, including maximum mean difference (MMD) and structure similarity index measure (SSIM). MMD is a statistical indicator used to measure the similarity between two probability distributions and evaluate the quality of generated samples [26]. A lower MMD value indicates a smaller distribution difference and higher generation quality. It is calculated by mapping samples to the reproducing kernel Hilbert space and computing the norm distance between the mean embeddings of two distributions. By mapping different samples to the kernel space, the norm distance is estimated. The closer the value is to 0, the higher the similarity between the two distributions. It is expressed as

$$\underset{GKC}{MMD}(RS, GS) = \left\| \frac{1}{m(m-1)} \sum_{i \neq j}^{m} k(rs_i, rs_j) + \frac{1}{n(n-1)} \sum_{i \neq j}^{n} k(gs_i, gs_j) - \frac{1}{mn} \sum_{i,j=1}^{m,n} k(rs_i, gs_j) \right\|_H^2, \quad (20)$$

where *RS* and *GS* represent the real data and generated sample, *GKC* is the generalized Gaussian kernel function, rs_i and gs_i are the *i*-th points from *RS* and *GS*, *k* is the Gaussian kernel function, *H* is the reproducing kernel Hilbert space.

By calculating the MMD for different samples under different working conditions, the quality of the generated sample is obtained, and it is shown in Table 3.

Table 3. The MMD for different cracked blades under different conditions.

Conditions	Health	Slight	Moderate	Severe
1200 rpm	0.68	0.71	0.73	0.75
1500 rpm	0.65	0.68	0.70	0.72
1800 rpm	0.66	0.69	0.71	0.73
2100 rpm	0.70	0.72	0.74	0.76
2400 rpm	0.72	0.74	0.76	0.78

Clearly, the MMD values at 1500 rpm and 1800 rpm are relatively low, and the reason is that the vibration signal characteristics are more stable at medium speeds, making it easier for the model to learn distribution patterns. The MMD value slightly increases at low speeds (1200 rpm) and high speeds (2400 rpm), where the signal fluctuates more strongly under extreme working conditions, which increases the difficulty of power generation. On the other hand, the MMD value gradually increases with the deepening of blade damage. This is because the fault pulse characteristics of severe damage are more complex and the signal is more non-stationary. However, the overall MMD value still remains around 0.7, and it indicates that the probability distribution of the samples generated by TCV_CGAN is highly consistent with the actual vibration signal distribution, which verifies the effectiveness of the proposed generation model.

In addition, the SSIM is employed to evaluate the generated sample quantitatively. Although the original SSIM algorithm is designed for two-dimensional images, a 1-D sliding-window implementation is adopted based on a local one-dimensional analysis window that slides along the time axis of vibration sequences. For each local window, luminance similarity, contrast similarity, and structural similarity are calculated. The final SSIM value is obtained by averaging all window-wise SSIM scores across the full-length time series [27].

Different from MMD, which mainly characterizes global probability-distribution discrepancy, 1-D SSIM focuses on local waveform-structure consistency. For turbine-blade vibration signals, fault-induced impact pulses and local oscillatory transients carry core diagnostic information. The 1-D SSIM can quantify the degree to which these key local waveform patterns are preserved in generated samples, providing complementary information to the distribution-oriented MMD metric. The value of SSIM ranges from 0 to 1. A value closer to 1 indicates higher structural consistency between generated and real vibration waveforms. It is expressed as

$$SSIM(RS, GS) = \frac{(2\mu_{RS}\mu_{GS} + C_1)(2\sigma_{RS,GS} + C_2)}{(\mu_{RS}^2 + \mu_{GS}^2 + C_1)(\sigma_{RS}^2 + \sigma_{GS}^2 + C_2)}, \quad (21)$$

where μ_{RS} and μ_{GS} represent the mean values of real and generated signal sequences, σ_{RS} and σ_{GS} are the standard deviations of the two signals, $\sigma_{RS,GS}$ is the covariance between real and generated samples for structural feature measurement, and C_1 and C_2 are constant terms to avoid a denominator of zero and ensure calculation stability.

By calculating the SSIM for different samples under different working conditions, the result is shown in Table 4. From the perspective of speed and damage degree, the performance of SSIM and MMD is basically the same. The SSIM values of the generated samples under all working conditions remain above 0.82, indicating that the structural

characteristics of the generated vibration waveform are highly consistent with the real signal, which further verifies the generation quality of the proposed TCV_CGAN.

Table 4. The SSIM for different cracked blades under different conditions.

Conditions	Health	Slight	Moderate	Severe
1200 rpm	0.92	0.89	0.87	0.85
1500 rpm	0.95	0.92	0.90	0.88
1800 rpm	0.94	0.91	0.89	0.87
2100 rpm	0.90	0.88	0.86	0.84
2400 rpm	0.88	0.86	0.84	0.82

Based on the evaluation results of MMD and SSIM, the proposed TCV_CGAN model not only achieves high consistency in global probability distribution, but also maintains good structural feature matching in local time-domain waveforms. The dual index evaluation fully verifies that the generated vibration samples have high fidelity, structural rationality, and adaptability to working conditions, effectively solving the problem of small sample size for turbine blade damage detection.

4.3. The Result of Turbine Blade Damage Detection

To further quantitatively verify the practical application effect of the proposed TCV_CGAN sample enhancement method in turbine blade damage detection, three evaluation indicators are employed to comprehensively evaluate the damage detection performance, including precision, recall, and F1 score. Precision represents the proportion of correctly predicted positive samples among all predicted positive samples, reflecting the classification accuracy of the model for each type. Recall refers to the proportion of correctly predicted positive samples among all actual positive samples, which characterizes the model's ability to detect all actual damaged samples. In addition, the F1 score is the harmonic mean of precision and recall, which comprehensively evaluates the overall detection performance of the model and avoids the one-sidedness of single indicator evaluation. Three indicators are calculated as

$$\begin{aligned} Precision &= \frac{TP}{TP + FP} \\ Recall &= \frac{TP}{TP + FN} \\ F1 &= \frac{2 \times Precision \times Recall}{Precision + \mathrm{Recall},} \end{aligned} \tag{22}$$

where TP is the true positive samples, FP is the false positive samples, and FN is the false negative samples.

To highlight the superiority of TCV_CGAN, the original unbalanced dataset and the balanced augmented dataset based on TCV_CGAN are separately analyzed under different working conditions. All experimental training and testing environments, network hyperparameters, and dataset segmentation ratios are kept completely consistent to ensure fairness and credibility of the comparison result, as shown in Figure 7.

Compared with the original imbalanced dataset, the balanced augmented dataset based on TCV_CGAN showed significant improvements in accuracy, recall, and F1 score under all speed conditions, with an average performance improvement of over 12%. This fully validates that the proposed sample augmentation method can effectively compensate for the shortage of actual fault samples and eliminate the adverse effects of imbalanced datasets on model detection performance.

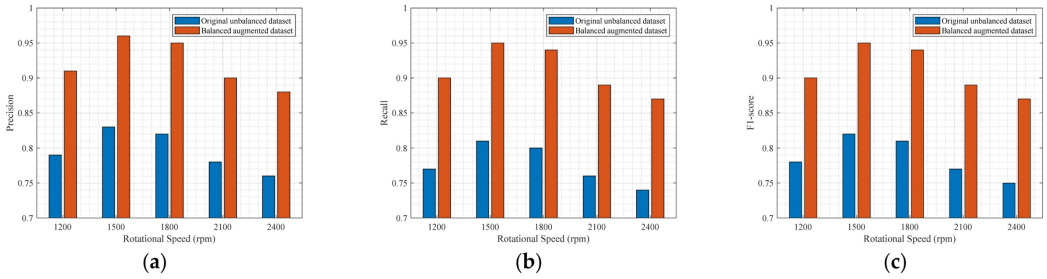


Figure 7. The result of blade damage detection under different conditions: (**a**) Precision. (**b**) Recall. (**c**) F1 score.

To further visualize the detection effect of the proposed method on different blade damage conditions and quantitatively analyze the misclassification situation, the confusion matrix is obtained based on the original unbalanced dataset and the balanced augmented dataset under the working condition of 1500 rpm. Both confusion matrices are calculated based on all 96 real test samples under this condition, and no generated samples are included in the test set. The number of samples in each category is inconsistent due to the natural class imbalance of the original dataset. The result is shown in Figure 8.

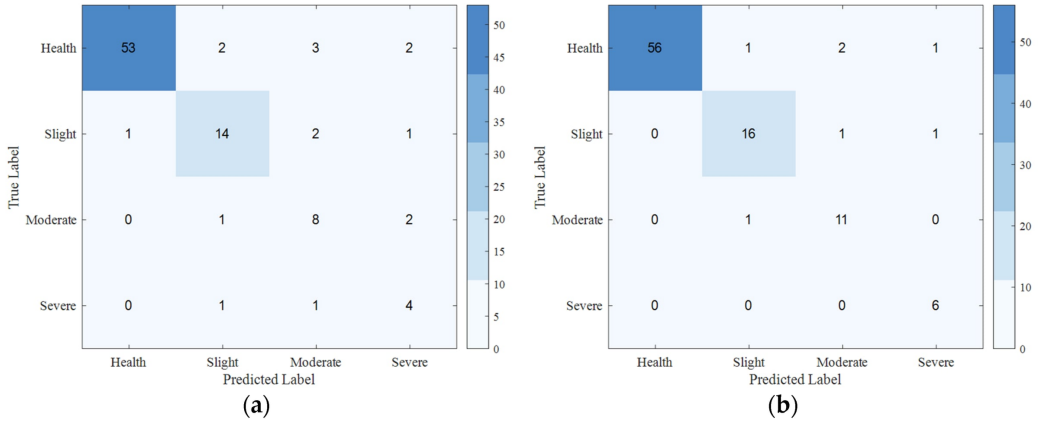


Figure 8. The confusion matrix of different datasets: (**a**) Original unbalanced dataset. (**b**) Balanced augmented dataset.

From the confusion matrix data, the original dataset has serious misclassification and missed classification problems, especially for samples with minor damage. Due to insufficient sample size and imbalanced class distribution, this model is prone to misidentifying minor damage signals as healthy signals, resulting in low detection accuracy for early weak faults. After using TCV_CGAN sample enhancement, the number of misclassified samples for all damage categories is significantly reduced. The classification accuracy of health status and mild damage has been greatly improved, and the misjudgment of moderate to severe injuries has been basically eliminated. The confusion matrix results further validate that the proposed TCV_CGAN method can effectively optimize the distribution of the dataset and provide reliable technical support for accurately detecting small sample faults in turbine blades.

4.4. Ablation and Comparative Analysis

The TCV_CGAN model is mainly composed of two core innovative modules, including the TCN and VCC modules. To verify the indispensable role of each module in improving sample generation quality and detection performance, a series of ablation experiments are designed to comprehensively verify the rationality of the model structure and its advanced

performance. The effectiveness of each key module of TCV_CGAN is demonstrated from different aspects. Three contrast model variants are set, including baseline CGAN (without TCN and VCC), CGAN with only the TCN module, and CGAN with only the VCC module. All experiments keep a consistent dataset, hyperparameters and training environment. After 10 rounds of averaging processing, the results are summarized in Table 5.

Table 5. The results of ablation analysis.

Model Structure	MMD	SSIM	Precision	Recall	F1-Score
Baseline CGAN	0.78	0.81	0.81	0.79	0.80
CGAN with TCN	0.71	0.88	0.87	0.86	0.86
CGAN with VCC	0.73	0.85	0.89	0.88	0.88
The proposed TCV_CGAN	0.68	0.92	0.96	0.95	0.95

Clearly, the single baseline CGAN model has the worst performance, with the highest MMD value, the lowest SSIM and detection indexes. It indicates that the traditional CGAN is prone to mode collapse and feature mismatch, resulting in low-fidelity generated samples and limited fault detection optimization effect. Compared with the baseline model, the model with a single TCN module achieves significant improvements in MMD and SSIM, which can capture long-range vibration fault features and improve the structural similarity between generated samples and real signals. It verifies that the TCN module can effectively expand the time-series receptive field. In addition, the model with a single VCC module obtains better detection accuracy, which proves that the VCC module can solve the problem of uncontrolled generation of traditional models and avoid label disorder and invalid sample generation.

To further verify that the generated samples accurately match the preset conditional attributes, quantitative validation is implemented from the perspectives of rotational speed and damage degree matching. The 1D CNN classifier is trained only with real samples under different rotational speed and damage degree conditions. The classification accuracy directly reflects the feature consistency between the generated samples and the target conditional attributes: higher accuracy indicates better controllable conditional generation performance of the model. After 10-fold cross-validation, the results are shown in Table 6.

Table 6. Quantitative validation for rotational speed and damage degree matching.

Rotational speed matching	**Health**		**Slight**	**Moderate**	**Severe**
	84.32%		83.69%	85.11%	86.47%
Damage degree matching	**1200 rpm**	**1500 rpm**	**1800 rpm**	**2100 rpm**	**2400 rpm**
	88.67%	89.02%	87.33%	88.14%	88.73%

The accuracy of rotational speed across all damage degrees and damage degree across all rotational speeds over 83.69% and 87.33%. Both maintain a relatively high level of conditional consistency, which confirms that the proposed multi-dimensional vector conditional encoding mechanism can effectively constrain the attribute characteristics of generated samples. The generated vibration signals are highly consistent with the preset damage states and rotational speed conditions, which verifies the effectiveness of the conditional encoding design.

Notably, the proposed TCV_CGAN model with dual modules achieves the optimal performance in all evaluation indicators. The complementary advantages of the two core

modules are fully reflected: the TCN module guarantees the time-domain structural authenticity of generated vibration samples, while the VCC module ensures the attribute accuracy and fine-grained generation capability. The collaborative optimization of the two modules fundamentally improves the quality of augmented samples and detection performance for cracked blades, which verifies the rationality and necessity of the proposed model structure.

To further demonstrate the superiority of the proposed TCV_CGAN method, five signal augmentation methods are employed for horizontal comparison, including traditional signal processing augmentation methods [12] and improved GAN-based generation methods of Vanilla GAN [28], traditional CGAN [29], TCN-GAN [30], and conditional WGAN [31]. Under the unified turbine blade small-sample dataset and detection framework, the sample generation quality and fault detection performance are compared for different methods. The results of the comparative analysis are shown in Table 7.

Table 7. The results of comparative analysis.

Model Structure	MMD	SSIM	Precision	Recall	F1-Score
Signal transformation augmentation	0.82	0.79	0.76	0.74	0.75
Vanilla GAN	0.79	0.82	0.80	0.78	0.79
Traditional CGAN	0.78	0.81	0.81	0.79	0.80
TCN-GAN	0.72	0.89	0.88	0.87	0.87
Conditional WGAN	0.74	0.86	0.85	0.84	0.84
The proposed TCV_CGAN	0.68	0.92	0.96	0.95	0.95

The comparison results show that traditional signal transformation augmentation methods have the worst overall performance. Simple amplitude scaling, noise addition and other linear transformation operations cannot mine the deep time-series fault features of blade vibration signals, resulting in low structural similarity and distribution consistency of augmented samples, which has limited improvement on small-sample fault detection. In addition, the original GAN and CGAN methods improve the data distribution to a certain extent, but lack targeted design for time-series vibration characteristics, resulting in frequent training oscillation and mode collapse. Specifically, TCN-GAN only focuses on time-series feature extraction and lacks multi-dimensional conditional constraints, which cannot realize fine-grained controlled generation, resulting in easy attribute confusion of generated samples. Conditional WGAN optimizes the loss function to improve training stability, but ignores the long-range temporal dependence of vibration signals, leading to insufficient feature extraction capability for weak early faults.

Compared with the improved TCN-GAN and conditional WGAN methods, the proposed TCV_CGAN method achieves the optimal performance in all indicators. It organically integrates temporal convolution feature extraction and multi-dimensional vector conditional supervision based on the composite loss function of adversarial loss and conditional matching loss. This design not only ensures the global distribution consistency and local structural authenticity of generated samples, but also realizes accurate matching of sample attributes and working conditions.

Compared with the existing optimal comparison method, the average F1-score of TCV_CGAN is improved by 8%, and the recognition accuracy of slight early damage is improved by more than 20%. It effectively solves the core problems of missed detection and misclassification of small-sample weak faults in turbine blade detection. Meanwhile, combined with the variable working condition experimental results, the proposed TCV_CGAN maintains stable and excellent generation and detection performance under different ro-

tational speeds and damage degrees, verifying its superior robustness and generalization ability in complex engineering scenarios.

5. Conclusions

The TCV_CGAN method is proposed to address the small sample and data imbalance problems in turbine blade fault diagnosis. Benefiting from the designed multi-dimensional VCC module and stacked dilated causal TCN module, the proposed method achieves fine-grained, high-fidelity directional generation of blade vibration signals under different damage degrees and variable rotational speed conditions. In addition, the constructed composite loss function integrates adversarial loss and conditional matching loss to stabilize model training, effectively avoiding conditional mismatch and mode collapse. To test the proposed method on sample augmentation and damage detection, the experimental turbine blade platform is established under different working conditions. Through the quantitative evaluation factors of MMD and SSIM, the performance of vibration sample augmentation is verified that the generated samples maintain high consistency of over 0.7 in both global probability distribution and local structural features, which can reach high accuracy of over 90% on crack detection for turbine blades. Combined with ablation and comparative analysis, the TCV_CGAN augmentation method significantly improves the precision, recall and F1-score of multi-degree blade damage identification, effectively reducing misclassification and missed detection of early weak faults and improving the detection performance for laboratory-simulated blade crack damage and enhancing the model's robustness across variable rotational-speed conditions within the experimental dataset. It should be noted that all damage cases in this work are artificially simulated cracks on a test rig. The generalization performance for naturally occurring in-service turbine-blade damage of different origins (such as fatigue cracks, wear, and corrosion) still requires further demonstration using real-world field data.

In future research, the TCV_CGAN framework will be further optimized by introducing adaptive kernel selection and multi-scale feature fusion modules to improve generation performance under strong noise and extreme working conditions. In addition, the frequency-domain feature consistency analysis is significant to quantitatively evaluate the generated samples under unseen rotational speed conditions. Moreover, the proposed data augmentation and detection framework can be extended to various rotating machinery equipment, which has broad application prospects for industrial intelligent fault diagnosis. Furthermore, future work will collect real-world turbine-blade vibration data with diverse natural damage origins to further verify the transferability and practical applicability of the proposed framework for industrial field scenarios.

Author Contributions: Conceptualization, J.X.; methodology, J.X. and J.W.; software, X.D.; validation, Z.L., D.D. and W.X.; formal analysis, J.X. and Z.W.; investigation, W.L. and J.X.; resources, Z.L.; data curation, D.D. and W.X.; writing—original draft preparation, J.X. and J.W.; writing—review and editing, W.L. and Z.W.; visualization, X.D.; supervision, Z.W.; project administration, J.W.; funding acquisition, J.W., D.D. and Z.L. All authors have read and agreed to the published version of the manuscript.

Funding: This research received no external funding.

Data Availability Statement: The original contributions presented in this study are included in the article. Further inquiries can be directed to the corresponding author.

Conflicts of Interest: Authors Jiamin Xu, Jianye Wang, Wangfan Li, Zhentian Wan, Xian Ding and Wangren Xu were employed by the Shanghai Power Equipment Research Institute Co., Ltd. Author Dongmei Dai was employed by the Nanjing Boxiang Information Technology Co., Ltd. The remaining

author declares that the research was conducted in the absence of any commercial or financial relationships that could be construed as a potential conflict of interest.

References

1. Marin, G.; Titov, A.; Akhmetshin, A.; Ishalin, A. Increasing the efficiency of a conversion gas turbine engine by adding hydrogen to fuel gas. *Int. J. Hydrogen Energy* **2025**, *97*, 649–656. [CrossRef]
2. Yang, H.; Ying, J.; Xue, J.; Lin, T.; Li, L.; Li, X.; Wei, Y.; Zhu, Z. Study on the energy acquisition mechanism of pump as turbine (PAT) under gas-liquid two-phase conditions. *Renew. Energy* **2026**, *256*, 123997. [CrossRef]
3. Cui, B.; Ahsan, S.; Zhang, J.; Liang, X. An improved Cox proportional hazards model for reliability analysis of aviation gas turbines considering varying environmental conditions and operational settings. *Reliab. Eng. Syst. Saf.* **2026**, *265*, 111451. [CrossRef]
4. Hadroug, N.; Iratni, A.; Hafaifa, A.; Alili, B.; Colak, I. Implementation of vibrations faults monitoring and detection on gas turbine system based on the support vector machine approach. *J. Vib. Eng. Technol.* **2024**, *12*, 2877–2902. [CrossRef]
5. Yan, J.; Zhang, M.; Sun, L.; Xie, Z.; Zhao, Z.; Zhang, J.; Wang, F. Shape sensing of a wind turbine tower based on a one-sided four-node quadrilateral inverse shell element with a coupling functional. *Thin-Walled Struct.* **2025**, *215*, 113577. [CrossRef]
6. Wong, B.; Fu, M. Unraveling of the statistical correlation between porosity, permeability and diffusivity of cold-sprayed Ti6Al4V. *J. Manuf. Process.* **2025**, *152*, 375–389. [CrossRef]
7. Luan, X.; Liu, X.; Lei, Z.; Zhao, J.; Sha, Y.; Guo, X. Fault feature extraction method for rolling bearing in gas turbine engines based on comprehensive dynamic screening. *Meas. Sci. Technol.* **2025**, *36*, 046116. [CrossRef]
8. Singh, G.; Schreiner, B.; Sun, X.; Sethi, V. A review of hydrogen micromix combustion technologies for gas turbine applications. *Int. J. Hydrogen Energy* **2025**, *127*, 295–310. [CrossRef]
9. Zhang, X.; Zhang, T. Practical semi-supervised learning framework for real-time warning of aerodynamic instabilities: Applications from compressors to gas turbine engines. *Reliab. Eng. Syst. Saf.* **2025**, *264*, 111261. [CrossRef]
10. Zhang, J.; Chang, X.; Xue, Y.; Bai, X.; Li, Z.; Wang, P.; Sun, H. Optimal planning for electricity–gas–hydrogen integrated energy systems considering intertemporal long-term hydrogen storage and multiple uncertainties. *IEEE Trans. Power Syst.* **2025**, *40*, 4660–4674. [CrossRef]
11. Jian, C.; Peng, Y.; Mo, G.; Chen, H. Open-set domain generalization for fault diagnosis through data augmentation and a dual-level weighted mechanism. *Adv. Eng. Inform.* **2024**, *62*, 102703. [CrossRef]
12. Ji, K.; Zhou, Z.; Li, Y. Vibration-based fault diagnosis of agricultural machinery: A review of field excitation, signal processing, intelligent models and engineering deployment. *Machines* **2026**, *14*, 795. [CrossRef]
13. Liu, Y.; Xu, Z.; Gao, F.; Zhao, J.; Song, C. Knowledge-driven compound fault detection enhancement based on multi-modal feature generative adversarial collaborative learning for industrial rotating machinery. *Mech. Syst. Signal Process.* **2026**, *244*, 113822. [CrossRef]
14. Nayak, A.; Venugopala, P.; Ashwini, B. A systematic review on generative adversarial network (GAN): Challenges and future directions. *Arch. Comput. Methods Eng.* **2024**, *31*, 4739–4772. [CrossRef]
15. Lin, C.; Kong, Y.; Huang, G.; Han, Q.; Dong, M.; Liu, H.; Chu, F. Generalization classification regularization generative adversarial network for machinery fault diagnostics under data imbalance. *Reliab. Eng. Syst. Saf.* **2025**, *256*, 110791. [CrossRef]
16. Zheng, D.; Chen, Y.; Ni, W.; Ye, J.; Wang, M.; Li, T. Physics-guided CGAN data augmentation method and applications in slug flowrates prediction based on ultrasonic sensors. *Measurement* **2026**, *290*, 122876. [CrossRef]
17. Wang, X.; Zhang, C.; Wang, Y.; Xu, Y.; Liu, Z.; Jiang, H. Fault diagnosis of rolling bearings with imbalanced samples using conditional temporal denoising diffusion generative adversarial network. *Measurement* **2026**, *283*, 122036. [CrossRef]
18. Wu, Z.; Wang, S.; Liu, C.; Wu, H.; Yi, J.; Pang, Y.; Cheng, G. A data augmentation method for shearer rocker arm bearing fault diagnosis based on GA-WT-SDP and WCGAN. *Machines* **2026**, *14*, 144. [CrossRef]
19. Ali, M.; Hu, H.; Wu, T.; Mansoor, M.; Luo, Q.; Zheng, W.; Jin, N. Segmentation of MRI tumors and pelvic anatomy via cGAN-synthesized data and attention-enhanced U-Net. *Pattern Recognit. Lett.* **2025**, *187*, 100–106. [CrossRef]
20. Slimane, A.; Kebdani, S.; Bouchouicha, B.; Benguediab, M.; Slimane, S.; Bahram, K.; Chaib, M.; Sardi, N. An interactive method for predicting industrial equipment defects. *Int. J. Adv. Manuf. Technol.* **2018**, *95*, 4341–4351. [CrossRef]
21. Tian, J.; Liu, H.; Gan, W.; Zhou, Y.; Wang, N.; Ma, S. Short-term electric vehicle charging load forecasting based on TCN-LSTM network with comprehensive similar day identification. *Appl. Energy* **2025**, *381*, 125174. [CrossRef]
22. Li, Q.; Ren, X.; Zhang, F.; Gao, L.; Hao, B. A novel ultra-short-term wind power forecasting method based on TCN and Informer models. *Comput. Electr. Eng.* **2024**, *120*, 109632. [CrossRef]
23. Jin, X.; Ji, Y.; Li, S.; Lv, K.; Xu, J.; Jiang, H.; Fu, S. Remaining useful life prediction for rolling bearings based on TCN–transformer networks using vibration signals. *Sensors* **2025**, *25*, 3571. [CrossRef] [PubMed]

24. Li, S.-G.; Chen, Q.-R.; Huang, L.; Chen, M.; Wei, C.-D.; Yue, Z.-J.; Liu, R.-X.; Tong, C.; Liu, Q. Data-driven approach to predict the fatigue properties of ferrous metal materials using the cGAN and machine-learning algorithms. *Adv. Manuf.* **2024**, *12*, 447–464. [CrossRef]
25. Fang, L.; Liu, S.; Cheng, F. Early micro-short circuit fault diagnosis of lithium battery pack based on Pearson correlation coefficient and KPCA. *Comput. Electr. Eng.* **2024**, *118*, 109481. [CrossRef]
26. Shi, H.; Cao, S.; Zuo, H.; Ma, J.; Lin, C. Deep subdomain adversarial network with self-supervised learning for aero-engine high speed bearing fault diagnosis with unknown working conditions. *Measurement* **2025**, *241*, 115668. [CrossRef]
27. Dehmer, M.; Redžepović, I.; Tratnik, N.; Pleteršek, P.Ž. A distribution-based framework for network similarity assessment. *Appl. Math. Comput.* **2026**, *531*, 130179. [CrossRef]
28. Yan, J.; Huang, H.; Yang, K.; Xu, H.; Li, Y. Synthetic data for enhanced privacy: A VAE-GAN approach against membership inference attacks. *Knowl.-Based Syst.* **2025**, *309*, 112899. [CrossRef]
29. Ba, Z.; Ma, Y.; Zhao, J.; Wang, F. Conditional generative adversarial networks for spectrum-compatible ground motion generation of scenario earthquakes. *Eng. Appl. Artif. Intell.* **2025**, *152*, 110755. [CrossRef]
30. Zhang, M.; Li, B.; Pei, Z.; Zeng, Y. A novel Transformer-Inception based GAN model for data augmentation to address class imbalance in water supply network leakage detection. *Measurement* **2026**, *290*, 122675. [CrossRef]
31. Yun, D.-J.; Jung, H.; Hwang, I.-J.; Kim, J.-H.; Lee, I.-H.; Hong, Y.-P.; Park, J. Conditional WGAN-GP-Based radome FSS inverse design for stealth applications. *IEEE Antennas Wirel. Propag. Lett.* **2025**, *25*, 821–825. [CrossRef]

Disclaimer/Publisher's Note: The statements, opinions and data contained in all publications are solely those of the individual author(s) and contributor(s) and not of MDPI and/or the editor(s). MDPI and/or the editor(s) disclaim responsibility for any injury to people or property resulting from any ideas, methods, instructions or products referred to in the content.